# Chapter 11

# Renal Diffusion-Weighted Imaging (DWI) for Apparent Diffusion Coefficient (ADC), Intravoxel Incoherent Motion (IVIM), and Diffusion Tensor Imaging (DTI): Basic Concepts

**Neil Peter Jerome, Anna Caroli, and Alexandra Ljimani**

## Abstract

The specialized function of the kidney is reflected in its unique structure, characterized by juxtaposition of disorganized and ordered elements, including renal glomerula, capillaries, and tubules. The key role of the kidney in blood filtration, and changes in filtration rate and blood flow associated with pathological conditions, make it possible to investigate kidney function using the motion of water molecules in renal tissue. Diffusion-weighted imaging (DWI) is a versatile modality that sensitizes observable signal to water motion, and can inform on the complexity of the tissue microstructure. Several DWI acquisition strategies are available, as are different analysis strategies, and models that attempt to capture not only simple diffusion effects, but also perfusion, compartmentalization, and anisotropy. This chapter introduces the basic concepts of DWI alongside common acquisition schemes and models, and gives an overview of specific DWI applications for animal models of renal disease.

This chapter is based upon work from the COST Action PARENCHIMA, a community-driven network funded by the European Cooperation in Science and Technology (COST) program of the European Union, which aims to improve the reproducibility and standardization of renal MRI biomarkers. This introduction chapter is complemented by two separate chapters describing the experimental procedure and data analysis.

**Key words** MRI, Kidney, Diffusion, Diffusion-weighted imaging (DWI), Apparent diffusion coefficient (ADC), Intravoxel incoherent motion (IVIM), Mouse, Rat

## 1 Introduction

The dominant role of magnetic resonance imaging (MRI), and in particular diffusion-weighted imaging (DWI), in the diagnosis and monitoring of renal disease is driven by the ability to provide simultaneous assessment of kidney anatomy and function. In addition to the potential to avoid or reduce the need for biopsy, which is invasive and subject to sampling bias, the use of functional imaging techniques such as DWI allow examination of tissue microstructure in vivo as well as the potential for challenge protocols using administered agents. In particular, in view of the controversial study on

Andreas Pohlmann and Thoralf Niendorf (eds.), *Preclinical MRI of the Kidney: Methods and Protocols*, Methods in Molecular Biology, vol. 2216, https://doi.org/10.1007/978-1-0716-0978-1_11, 

gadolinium-containing MR contrast agents with regard to nephrogenic systemic fibrosis (NSF) [1] or possible gadolinium deposits in the central nervous system (CNS) [2], contrast-free examination techniques are to be preferred, especially in patients with impaired renal function.

Diffusion-weighted imaging comes in many variants, from simple to complex schemes, all based on indirect observation of water molecular motion, that are sensitive to changes in renal perfusion and tubular flow, alterations of cellularity arising from inflammation, edema, or hyperplasia, and from fibrosis. A recent review of the application of renal DWI in humans [3] gives an overview of research performed so far and illustrates renal DWI potential in the clinic. The authors in particular conclude that DWI is well-placed to investigate decline of renal function as well as to monitor disease progression in both acute and chronic kidney diseases, while noting that complexity of the diffusion signal makes biological validation difficult.

The strengths of DWI are not without accompanying drawbacks, however, which include the relatively long acquisition times required for advanced DWI protocols, an increased susceptibility to image artifacts, and an overall decreased spatial resolution due to the imaging sequences used. Careful consideration of both the research question to be addressed and the optimal acquisition parameters to be used, together with acquisition of complementary MRI modalities, can ameliorate some of these issues.

This chapter discusses the underlying phenomena and contrast mechanisms of diffusion-weighted imaging. It is complemented by two separate chapters describing experimental procedure and data analysis, which are part of this book.

This chapter is part of the book Pohlmann A, Niendorf T (eds) (2020) Preclinical MRI of the Kidney—Methods and Protocols. Springer, New York.

## 2 Diffusion Weighted Imaging Concepts

### 2.1 Fundamental Concept

MRI signal arising from water protons in vivo is sensitive to the exact nature of the tissue, including not only how the spins interact with the tissue lattice and other spins through $T_1$ and $T_2$ relaxation mechanisms, but also the tendency of water molecules to physically move around, or diffuse, over time. The use of the term diffusion-weighted imaging is a general catch-all term for any imaging using pulsed field gradients for motion sensitization. DWI is sensitive to the nature and degree of proton movement, which depends on tissue microstructure, therefore representing an informative component of research and clinical MRI protocols.

The use of pulsed gradient fields added to a MRI readout sequence, in a dephase-rephase cycle commonly implemented as a polarity-reversed pair or as equal pulses placed either side of a spin-echo pulse, causes a loss of the MRI signal proportional to the

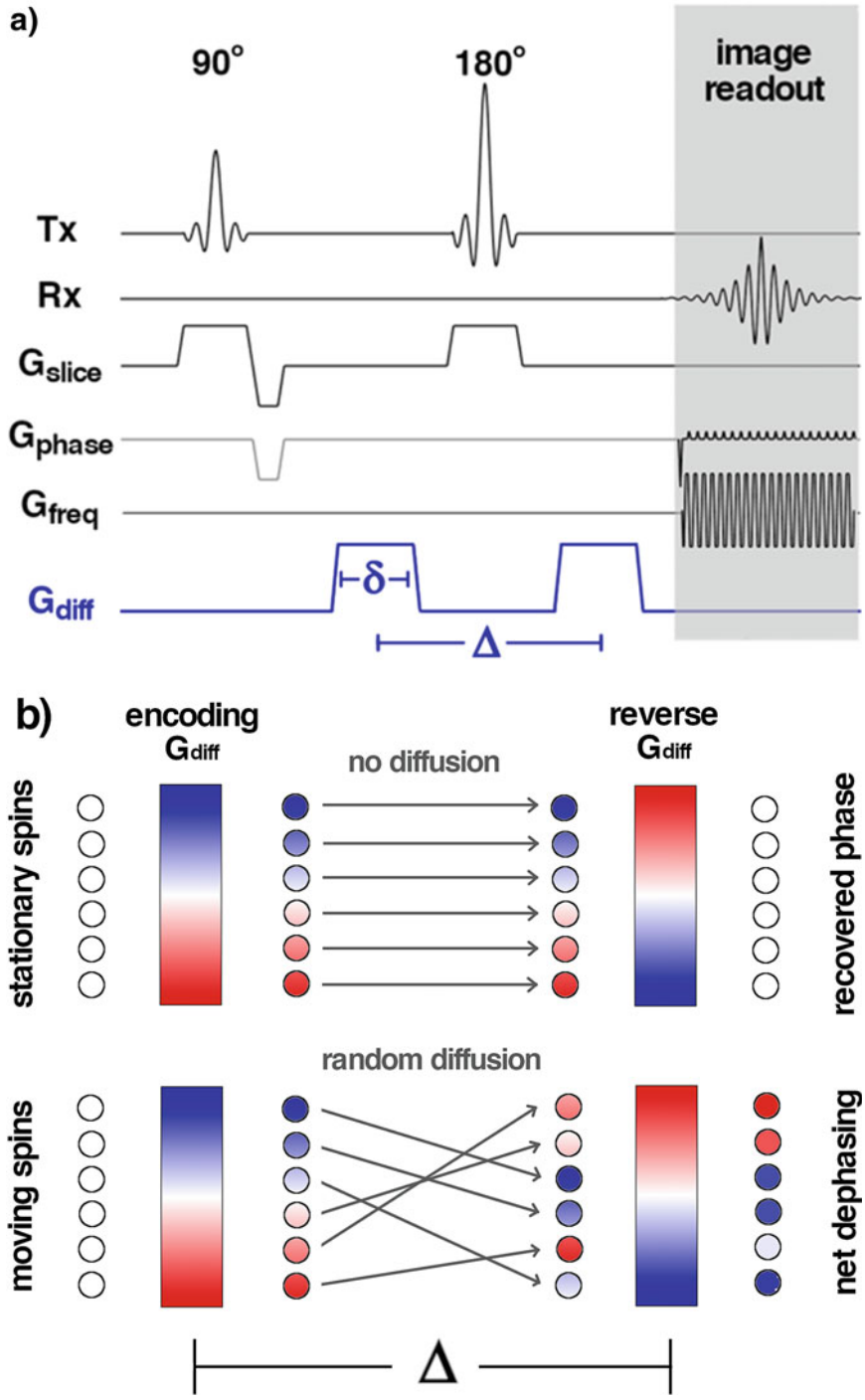


**Fig. 1** Illustration of (**a**) DWI pulse sequence, showing the diffusion gradients (lower line, in blue) for a spin-echo echo-planar readout sequence. (**b**) Schematic one-dimensional illustration of the net dephasing of spins dependent on their motion. The initial gradient pulse adds an additional phase (red and blue being +/− additions to the static magnetic field) by transiently modulating the Larmor frequency of the spins. The amount of additional phase is defined by the spin location along the gradient pulse direction (here up/down for simplicity). During the diffusion time $\Delta$, spins have an opportunity to diffuse according to their tissue environment. The reverse pulse (in practice the same polarity, but acting as reversed in combination with the 180° spin-echo pulse) restores the phase offset for spins that have not moved (upper section), whereas moving spins do not receive equal dephase and rephase shifts, leading to a net phase shift (indicated by remaining color) and an overall signal loss

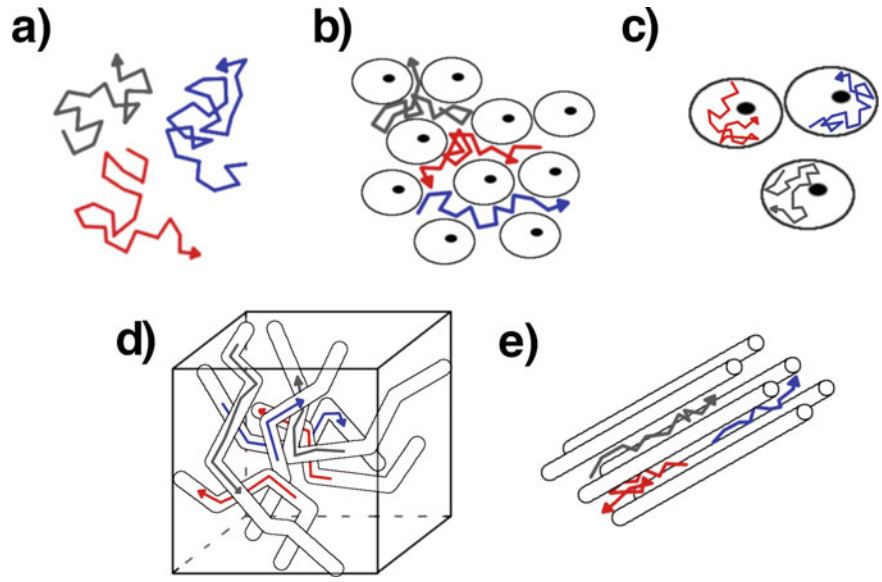


**Fig. 2** Schematic summary of motion types that can be investigated by diffusion imaging. Illustrative paths for water molecules are shown for: (**a**) free diffusion, also called Gaussian or true diffusion, that is a random motion; (**b**) apparent hindered diffusion in the tissue, where the microstructure alter true diffusion by introducing barriers; (**c**) apparent diffusion restriction, for example within cells (**d**) pseudodiffusion, denoting motion due to flow in vessels or tubules; and (**e**) diffusion directionality caused by structural elements

overall mis-match of the pulses experienced by spins that have changed location (Fig. 1). The larger the distance covered by water molecules (and the proton spins therein) between the gradient pulses, the greater the mismatch of pulses experienced by the spins, and the greater the overall signal destruction from the net spin dephasing. Over time, this basic DWI concept has been implemented into a raft of specialized sequences, targeted and optimized for different applications.

### *2.2 Water Motion and Relation to Microstructure*

In a large, single-compartment system, free diffusion of water molecules is a truly chaotic, random phenomenon known as Brownian motion, and might go on indefinitely (Fig. 2a). Here, the average displacement of molecules over time is described by an increasingly wide distribution, Gaussian (or normal) in nature, centered on the starting position and characterized by a *diffusion coefficient*. In biological tissues, water molecules interact with surrounding structures (cell walls, extracellular matrix, and so forth), which act as barriers causing an alteration and possible restriction in diffusion (Fig. 2b, c). Tissue microstructure may also contain flow elements, or structure with directional preference (Fig. 2d, e). The observed diffusion coefficient from an imaging voxel, which may contain a complex mix of diffusion environments, is thus an empirical parameter, the *apparent diffusion coefficient (ADC)* measured in $mm^2/s$. Since tissue microstructure is a major determinant of apparent diffusion, pathological conditions affecting microstructure cause an alteration in ADC.

The length scale of diffusion imaging, that is the average distance covered by water molecules during the DWI experiment, is determined as a balance of the average speed of the water molecules in their environment and the diffusion time allowed in the acquisition. Moreover, it is possible to see signal characteristic of molecules whose motion is restricted to certain structures if the length scale exceeds the structure dimensions. This, for example, allows for the inference of intracellular water motion and thus cell size in appropriately designed DWI protocols [4].

In the kidney, nonrandom perfusion and tubular flow, which manifest as pseudodiffusion processes, as well as the high degree of directional order in the renal structure, add complexity to the investigation of water molecule motion. Specific signal interpretation models have been developed to account for an additional (or sometimes more than one) pseudodiffusion compartment, generally possessing a pseudodiffusion coefficient of a higher magnitude than that of true diffusion. Similarly, additional models assessing diffusion along multiple explicit directions have been developed to provide information on directional motion as well as on the relative anisotropy of the tissue.

Since the complexity of diffusion signal interpretation models is intrinsically tied to the complexity of image acquisition protocols, DWI acquisition and analysis cannot be considered and discussed independently (*see* **Note 1**). The choice of acquisition parameters will determine and/or limit the possible signal interpretation models, and therefore acquisition must be carefully designed, with the expected analysis in mind. In particular, DWI acquisitions are often lengthy, and there is always pressure to limit their duration when transferred to clinical practice to minimize patient discomfort. When planning renal DWI studies in the preclinical setting, it is thus important to consider also their translational potential, and the additional value that more complex acquisitions offer in relation to the extra scan time required.

## 3 Diffusion Modeling

The degree of diffusion weighting applied to an image is conventionally reported as its *b*-value, where *b* is a compound parameter, expressed in $s/mm^2$, arising from the specifics of the pulsed gradients used to sensitize the signal to spin motion. The *b*-value is limited by the gradient hardware, but values of several thousand are commonly achievable. Given that the incomplete rephasing of displaced water molecules explicitly leads to a loss of signal, increased diffusion weighting is ultimately limited by signal-to-noise and in general is performed with a lower spatial resolution than images acquired using other MRI modalities. Sufficiently high *b*-values may reduce the signal to the level of background noise, and in these cases either these data can be excluded, or an explicit noise term added to the analysis.

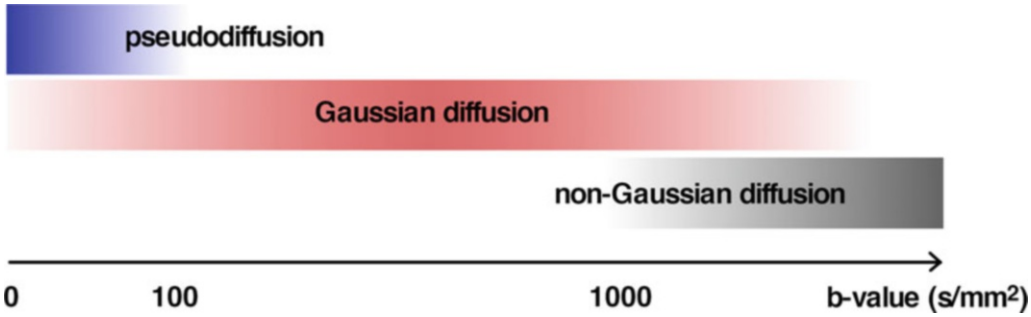


**Fig. 3** Different diffusion weightings, summarized by the compound parameter *b*-value, give rise to diffusion signal that is influenced by different diffusion regimes. Intuitive, though necessarily simplified, interpretations of these diffusion phenomena include (1) pseudodiffusion, observed at low *b*-values and reflecting vessel and tubular flow; (2) Gaussian (or random) diffusion, reflecting diffusion of water molecules in the renal tissue and thus informing on renal microstructure and cellularity; and (3) non-Gaussian diffusion, observed at high *b*-values and providing additional information on tissue microstructure. In addition to *b*-value, diffusion time, delay, and direction parameters influence the observed DWI signal

The range of *b*-values used in a diffusion imaging protocol defines which diffusion components will be present and/or dominate the signal, and thus will influence the analysis. The simplified illustration in Fig. 3 gives a rough guideline to the *b*-value ranges where different diffusion phenomena can be detected, though it is important to appreciate the simplifications made when attempting to model diffusion processes in tissue, and that *b*-value magnitude alone is not sufficient to describe the experiment.

In some circumstances, such as the spatial localization of tumors, it may be sufficient to simply observe the hyperintense signal of highly cellular regions on a single diffusion-weighted image of sufficient *b*-value to provide increased contrast (although at lower overall signal). Diffusion-weighted images have an underlying $T_2$ weighting arising from the longer TE required to allow for inclusion of the diffusion-sensitizing pulses, which can be confounding where long-$T_2$ regions (e.g., free water) can be mistaken for low diffusion areas—this is known as the $T_2$ *shine-through* effect [5]. In most applications, however, modeling of the DWI signal behavior, across a set of matched images varying only in the applied *b*-values, removes the $T_2$ influence and gives quantitative parameters that are, in theory, comparable across studies (*see* **Note 2**).

In the following sections, several diffusion signal interpretation models relevant to renal studies are described, though this is far from an exhaustive list of models or mathematical representations available. Choice of DWI protocols are often selected in terms of the additional value that they may offer in relation to their additional complexity and duration, and with a particular diffusion model and analysis scheme in mind (*see* **Note 3**).

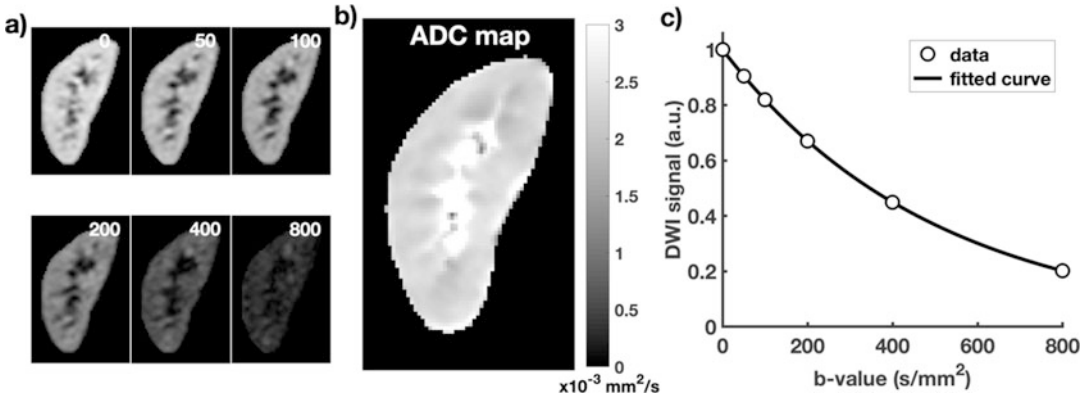


**Fig. 4** Monoexponential ADC model. (**a**) Example DWI images acquired with different *b*-values (given in s/mm$^2$) from a healthy kidney, and (**b**) the ADC map resulting from fitting a monoexponential model. Signal-to-noise ratio, depending on $T_2$, spatial resolution, and the underlying diffusion itself, decreases with the increase in *b*-value. (**c**) Schematic illustration of an ideal ADC curve fit to noiseless data. Analysis methods are discussed in detail in the chapter by Jerome NP et al. "Analysis of Renal Diffusion-Weighted Imaging (DWI) Using Apparent Diffusion Coefficient (ADC) and Intravoxel Incoherent Motion (IVIM) Models"

### *3.1 Monoexponential Apparent Diffusion Coefficient (ADC)*

The simplest and most widely used model to interpret the DWI signal is a single compartment model, summarizing all motion components (from diffusion, flow, etc.) in a single coefficient (ADC, *see* **Note 4**). The resulting ADC maps (*see* Fig. 4) are derived from the fitting of the DWI signal, across all *b*-values on a voxel-wise basis, of a single-exponential model according to the following formula:

$$S_{(\mathrm{b})} = S_{(\mathrm{total})} . \exp\left(-\frac{\mathrm{TE}}{T_2}\right) . \exp\left(-b.\mathrm{ADC}\right) \qquad (1)$$

where $S_{(\mathrm{b})}$ and $S_{(\mathrm{total})}$ represent the signal observed at a particular *b*-value, and the overall equilibrium signal (at $b = 0$ s/mm$^2$ and TE = 0 ms) respectively. Since the echo time TE is usually not varied across images with different diffusion weightings, the first two terms are often summarized as $S_0$, the signal at a *b*-value of zero, and the formula simplifies as follows:

$$S_{(\mathrm{b})} = S_0 . \exp\left(-b.\mathrm{ADC}\right) \qquad (2)$$

Despite the DWI signal not being truly monoexponential, and ADC being a purely empirical parameter summarizing different factors contributing to the diffusion signal, ADC can still be considered as a sensitive and useful biomarker [6, 7].

The monoexponential model requires acquisition of a minimum of 2 *b*-values. The lower value is commonly set as zero by default, although this leads to what is known as a perfusion-sensitive ADC; choosing a minimum *b*-value of approximately

100–200 s/mm$^2$ removes this influence to give a perfusion-insensitive ADC. The highest *b*-value is normally chosen as the maximum value while retaining sufficient signal, commonly in the range 700–1000 s/mm$^2$ [8], although non-Gaussian processes may become relevant at this upper limit (Fig. 3). The coefficient derived from the analysis is always referred to as ADC, although it is important to note that if the underlying signal curve is not mono-exponential the measured ADC strongly depends on the *b*-values chosen [9], and so is not necessarily comparable across studies. Main advantages of the simple monoexponential equation is the short acquisition time required, and the general robustness of ADC as a marker of diffusion [10]. The monoexponential model is also suited to DWI studies with multiple *b*-values, with additional data points allowing for estimation of ADC uncertainties.

### 3.2 Intravoxel Incoherent Motion (IVIM)

One advanced model to interpret the diffusion imaging signal is the intravoxel incoherent motion (IVIM) model. Originally proposed by Le Bihan for the assessment of microcapillary perfusion in the brain [11], the model is generally applicable if a number of assumptions are fulfilled, and represents a popular choice for attempting to separate diffusion from flowing components [12].

In this model, a second compartment is included in the signal interpretation to describe the flow-based motion of water molecules in blood capillaries and tubules that, if assumed to randomly occur in all directions, appears as an accelerated diffusion process (Fig. 5).

The pseudodiffusion component associated with flow is described by the pseudodiffusion coefficient $D^*$ that, since flow is faster than diffusion, is approximately an order of magnitude larger

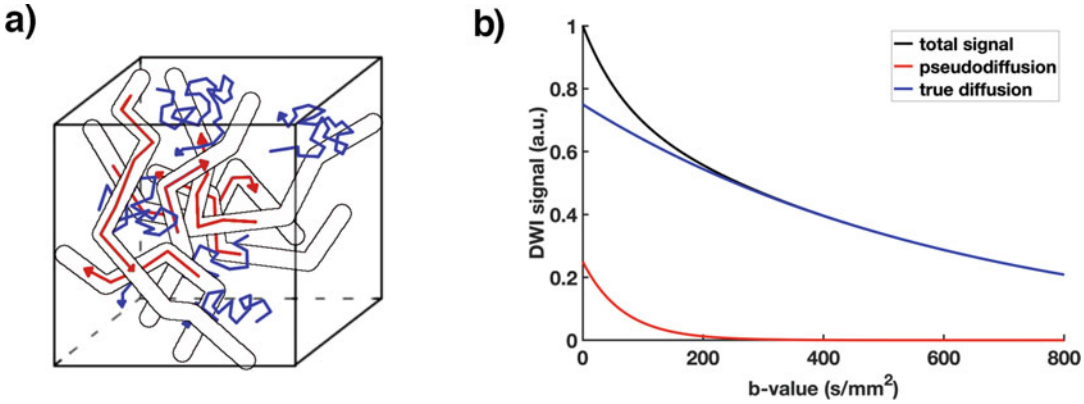


**Fig. 5** IVIM model. (**a**) Schematic representation of random water motion in a voxel of renal tissue, where free diffusion component (in blue, described by the diffusion coefficient *D*) is complemented by fluid flowing in capillaries and tubules (in red, described by the pseudodiffusion coefficient *D**). (**b**) Contributions of true diffusion and pseudodiffusion to the observed diffusion signal decay—pseudodiffusion is substantially faster than true diffusion, and so is only observed at low *b*-values

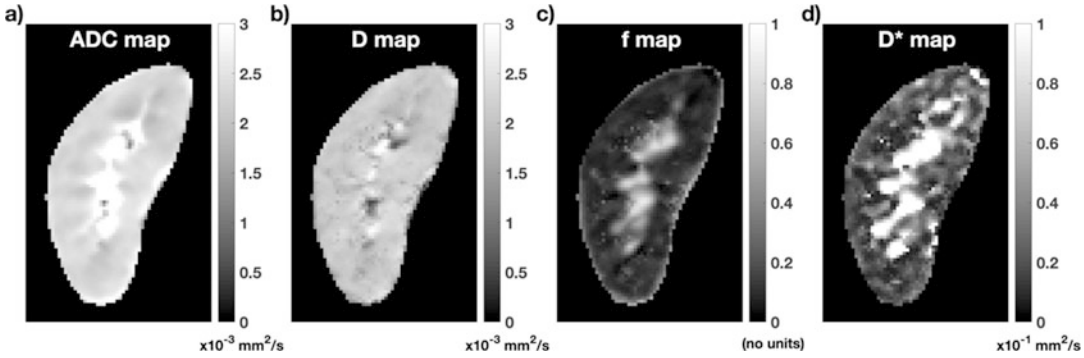


**Fig. 6** Representative parametric maps resulting from DWI model fitting. (**a**) ADC map, resulting from monoexponential model fitting. (**b**) Pure diffusion *D*, (**c**) pseudodiffusion fraction *f*, and (**d**) pseudodiffusion *D** maps, resulting from IVIM model fitting over several *b*-values. DWI-based parameters show contrast between the cortex, medulla, and renal hilum. Some extreme values are seen as a consequence of respiratory motion at the lower boundary of the kidney. Parameters associated with pseudodiffusion, *f* and *D**, commonly give maps with higher noise

than the true diffusion coefficient *D*. The components have relative signal contributions given by the pseudodiffusion fraction ($f$), and the overall IVIM model is described by the following equation:

$$S_{(b)} = S_0.((1-f).\exp(-b.D) + f.\exp(-b.D^*)) \qquad (3)$$

implicitly assuming that there is no exchange between the compartments, and that the associated compartmental $T_2$ values are the same. Since this is known not to be true in certain circumstances [13, 14], it is important to note that the derived pseudodiffusion coefficient $D^*$ and pseudodiffusion fraction $f$ are nevertheless empirical and should strictly be considered reflective of and not, as often stated, a direct measure of perfusion or flow.

The use of the IVIM model requires substantially more complex analyses than the monoexponential model (analyses are discussed in the chapter by Jerome NP et al. "Analysis of Renal Diffusion-Weighted Imaging (DWI) Using Apparent Diffusion Coefficient (ADC) and Intravoxel Incoherent Motion (IVIM) Models"), and more care to reliably separate pure diffusion from pseudodiffusion components. IVIM analysis tools are increasingly being offered by MRI manufacturers, although the choice of model fitting methods may significantly influence the derived parameters from the more complex model [15, 16]. Parametric maps resulting from IVIM analysis show the similarity of *D* coefficient with ADC, and the increased noise that is characteristic of the pseudodiffusion parameters *f* and *D** (Fig. 6).

The main feature of any DWI acquisition intended for IVIM analysis is the increased number of *b*-values required, especially low *b*-values that sample the signal curve before the pseudodiffusion component has decayed (Fig. 5). Simplified versions of the IVIM

approach usually attempt to limit the acquisition time by using fewer *b*-values, the minimum being three for a segmented fitting that does not attempt to measure $D^*$ [15, 17–19]. Additional complications of multiple *b*-value acquisitions are the increased sensitivity to movement, and the known difficulty of providing repeatable pseudodiffusion parameters compared to diffusion [20–22].

### 3.3 Diffusion Tensor Imaging (DTI)

If the directionality (or loss thereof) of diffusion arising from tissue structure is of interest, for example as an indication of loss of function or invasion of relevant tissue, consideration of the diffusion signal decay along specified direction, expressed as a tensor, allows calculation of an ellipsoid that represents the diffusion propagator in three dimensions. In the simplified case of isotropic diffusion, diffusion is equal in all directions and the ellipsoid is a sphere. Diffusion isotropy is assumed, though often unstated, in both the monoexponential and IVIM models described above. Conversely, in diffusion tensor imaging (DTI), diffusion-sensitizing gradients are applied along a number of prespecified directions, which are included in the model used to interpret the diffusion imaging signal. In DTI, the diffusion is assumed to be Gaussian and to follow a monoexponential signal decay.

The degree of direction-dependency of the diffusion signal is captured by the fractional anisotropy (*FA*) parameter, ranging from 0 (complete isotropy) to 1 (complete anisotropy) and derived from the relative dimensions of the diffusion ellipsoid according to the following equation:

$$\mathrm{FA} = \sqrt{\frac{3\left[(\lambda_1 - \mathrm{MD})^2 + (\lambda_2 - \mathrm{MD})^2 + (\lambda_3 - \mathrm{MD})^2\right]}{2\left({\lambda_1}^2 + {\lambda_2}^2 + {\lambda_3}^2\right)}} \tag{4}$$

where $\lambda_i$ represent the eigenvalues of the corresponding diffusion eigenvectors, meaning diffusion coefficients along each of the principal ellipsoid axes, and MD represents mean diffusivity, given by the following:

$$\mathrm{MD} = (\lambda_1 + \lambda_2 + \lambda_3)/3 \tag{5}$$

Directional diffusion coefficients can be reported for each individual direction ($\lambda_i$) or along the major and minor axes of the ellipsoid ($\lambda_1$ and $\lambda_{trans}$, the latter computed as average of the transverse axes coefficients). Given their complexity and alternative formulations, DTI equations used in any study should be clearly stated [23, 24].

Similar to IVIM, DTI requires the acquisition of substantially more images than the basic DWI scheme, although for DTI the number of directions of the applied diffusion-sensitizing gradients is increased rather than the number of *b*-values. In order to define

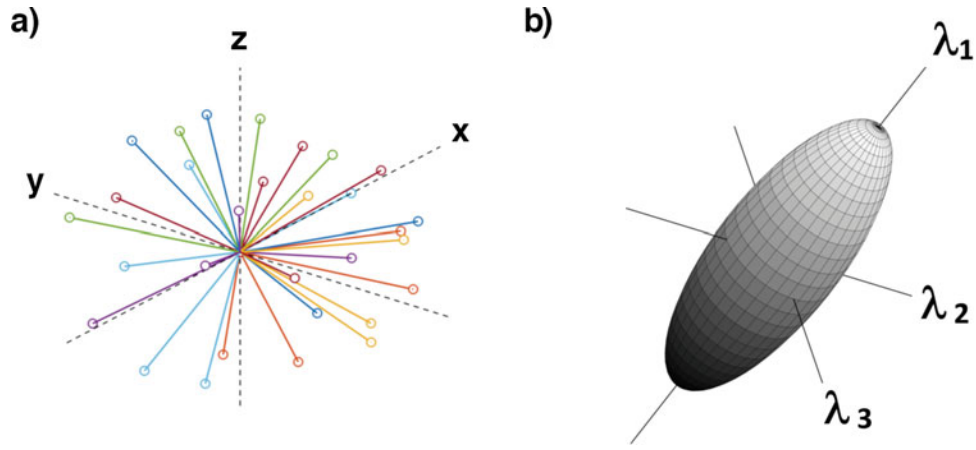


**Fig. 7** Illustration of diffusion tensor imaging principles. (**a**) Diffusion vectors in q-space, representing diffusion gradients of equal magnitude applied along different directions (in this case $n = 30$) to investigate tissue anisotropy. (**b**) Corresponding diffusion propagator ellipsoid, where $\lambda_i$ represent diffusion magnitude along each of the principal ellipsoid axes (i.e., eigenvalues of the principal eigenvectors). Measures of anisotropy, derived from these eigenvalues, are able to describe diffusion with directional preference

the tensor, a minimum of six different directions must be acquired alongside the $b = 0$ image (which, not being diffusion-weighted, has no directionality), but to reduce noise sensitivity it is common to acquire more, up to 30 or even 60 directions. Diffusion directions are usually equally distributed over the surface of a sphere, forming a "shell" in diffusion space (also called q-space), although user-defined vector sets are acceptable as long as there is sufficient sampling of the diffusion directions (Fig. 7).

The DTI technique was developed for application in the brain, but can provide relevant information in the kidney as well. Color and brightness of fractional anisotropy maps indicate orientation and degree of anisotropic diffusion, and can be portrayed as small ellipsoids, which are oriented and color-coded according to the direction of strongest diffusion, to illustrate tissue structure (similar to tractography in brain white matter). Maps of mean diffusivity resemble conventional diffusion coefficient maps (Fig. 8).

Given the large number of images required for DTI analysis, it is common to acquire only one shell in q-space, corresponding to a single non-zero *b*-value chosen based on the target tissue and expected signal-to-noise ratio. For body applications, this is much lower than for the brain, and is commonly within the range 500–1000 s/mm$^2$. More complex acquisition strategies are available, including multiple shells, as well as the option to retroactively ignore the directional information and calculate ADC.

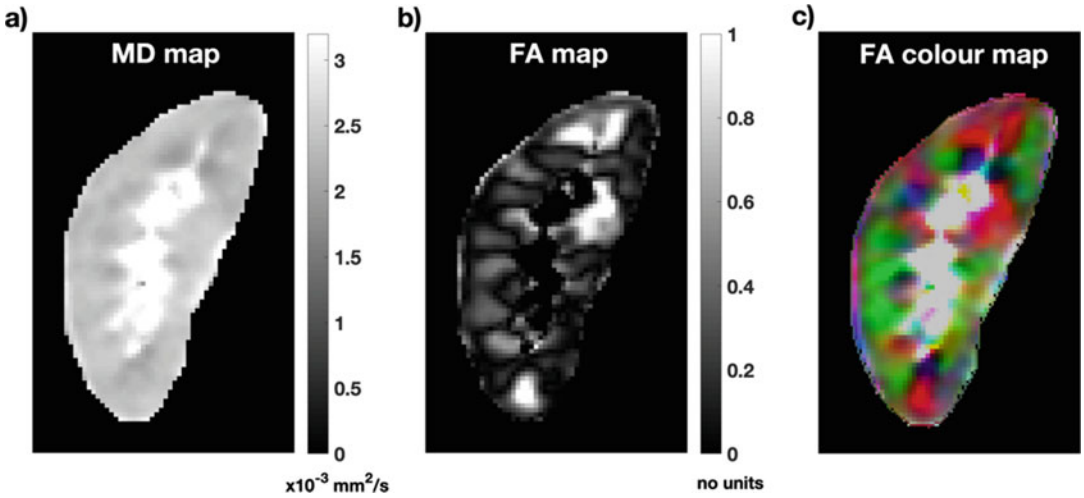


**Fig. 8** Representative parametric maps resulting from diffusion tensor imaging analysis of a healthy kidney. (**a**) Mean diffusion (MD) map. (**b**) Fractional anisotropy (FA) map in gray scale. (**c**) FA map in color scale, illustrating the direction of the $\lambda_1$ eigenvector

## 4 Diffusion Imaging in the Kidney

A more detailed review of the applications of renal diffusion imaging in humans was recently conducted by the international COST Action PARENCHIMA [3]. Much of the literature summarized therein, predominantly using the most established ADC but also including IVIM and DTI measures, reports a correlation between diffusion metrics and eGFR decline [25–29] or fibrosis [30–32], in patients with diabetes and other chronic kidney disease (CKD) [33–38], as well as in kidney allograft recipients [30, 39, 40].

Preclinical studies also demonstrate the broad connection of ADC with renal disease, with both ADC and DTI studies having links to renal fibrosis from acute ureteral obstruction [41–45] and diabetes [46, 47]. Preclinical studies also allow for study of the effects of potential contrast agents [48–50]. The development of novel DWI-based biomarkers may yet rely on biological validation and an improvement in specificity [51].

## 5 Diffusion Acquisition Considerations

In diffusion imaging, most trade-offs are about keeping the acquisition time reasonable and, similar to other MRI modalities, acquiring signal-to-noise ratio sufficient to provide reliable results. Preclinical imaging protocols are less constrained by time than clinical protocols, and so allow for longer scanning that may take advantage of increased averaging or alternate acquisition schemes.

Since increasing the number of acquired averages to give sufficient signal-to-noise quickly becomes prohibitive, DWI is normally acquired with lower spatial resolution than anatomical $T_1$- or $T_2$-weighted images. Number and repeats of each *b*-value depend on time available and intended analysis strategy, and are thus specific to each study and/or scanner. By default, most MR scanners will acquire three orthogonal directions (which may or may not be available as separate images [52]) for all nonzero *b*-values in order to calculate the *trace image*, implicitly assuming isotropic diffusion. Such schemes ultimately determine the exact sampling and thus the format of the resulting data. Furthermore, most diffusion imaging sequences allow for specification of several diffusion schemes (often with vendor-specific names and implementations), which trade-off between image quality and diffusion direction specifics. Such schemes may involve multiple "shots" to acquire k-space [31, 53], smaller field-of-view excitation through combination pulses [54], as well as variations on the gradient scheme such as bipolar encoding, designed to reduce distortion from eddy currents [55, 56]. In general, diffusion-weighted images may require an explicit postprocessing protocol as part of the analysis (*see* **Note 5**).

Since the acquisition of high *b*-values requires a larger TE in order to accommodate the pulses, the choice of the maximum *b*-value is a compromise between precision of diffusion estimates over a suitably chosen *b*-value range, and the available signal (*see* **Note 6**). DWI sequence variants that explicitly probe the effects of the diffusion time $\Delta$ as well as TE illustrate the importance of not neglecting potential influences of the acquisition parameters on the diffusion signal [13, 57].

Other significant factors in diffusion imaging arise directly from the use of echo-planar imaging (EPI) readout sequences, which although suitably fast gives images which are susceptible to distortion artifacts arising from high use of gradients (finite slew rates, eddy currents, nonlinearity, and so forth) and local susceptibility differences at tissue boundaries (and especially at tissue–air boundaries). Distortion correction can thus be necessary in diffusion imaging, and may involve prospective planning (e.g., phase-reversal images) [58] as well as retrospective processing (e.g., registration) [59].

Additional DWI protocols, such as those including flow compensation [60], alternate strategies to EPI readout [53, 61], and steady-state free precession sequences [62–64] and the influence of physiological factors on the DWI [65], have been reported in literature and may provide tools for ameliorating specific physiological and instrumental factors.

## 6 Notes

1. The specifics of diffusion imaging data acquisition and intended analysis strongly influence each other, and thus both should be borne in mind while planning a new study. Whenever possible, overly specific acquisition protocols should be avoided to allow for data reuse through additional retrospective analysis, and cross-study comparisons.
2. Many acquisition parameters influence the resulting diffusion-related parameters, making comparison across studies challenging. In the absence of widely accepted standardized protocols, it may be advantageous to consider the extent to which comparison with other studies will be possible.
3. As with all MRI studies, but of particular importance in diffusion imaging, care should be taken to report the adopted protocol as completely as possible. This necessarily includes the acquisition scheme and parameters, but also extends to the analysis algorithms.
4. The majority of diffusion models contain a parameter that attempts to capture the underlying tissue diffusion—ADC, (IVIM) *D*, (DTI) MD, and so on. While superficially similar and reflective of tissue structure, they are not precisely equivalent given the different assumptions implicit in the models they derive from.
5. The most common readout for diffusion imaging is the echo planar imaging (EPI) sequence, which is susceptible to artifacts and distortion; an adequate post-processing scheme is required. Analysis of DWI is discussed in more detail in the chapter by Jerome NP et al. "Analysis of Renal Diffusion-Weighted Imaging (DWI) Using Apparent Diffusion Coefficient (ADC) and Intravoxel Incoherent Motion (IVIM) Models."
6. Since diffusion contrast is created by deliberate dephasing and thus loss of the MR signal, sufficient signal-to-noise ratio is critical to ensure good quality data and successful analysis. Failure to assess the signal-to-noise ratio or account for the noise floor may introduce bias in the estimate of diffusion parameters.

## Acknowledgments

NPJ wishes to acknowledge support from the liaison Committee between the Central Norway Regional Health Authority and the Norwegian University of Science and Technology (Project nr. 90065000).

This chapter is based upon work from COST Action PARENCHIMA, supported by European Cooperation in Science and Technology (COST). COST (www.cost.eu) is a funding agency for research and innovation networks. COST Actions help connect research initiatives across Europe and enable scientists to enrich their ideas by sharing them with their peers. This boosts their research, career, and innovation.
PARENCHIMA (renalmri.org) is a community-driven Action in the COST program of the European Union, which unites more than 200 experts in renal MRI from 30 countries with the aim to improve the reproducibility and standardization of renal MRI biomarkers.

## References

1. Roditi G, Maki JH, Oliveira G, Michaely HJ (2009) Renovascular imaging in the NSF era. J Magn Reson Imaging 30:1323–1334
2. Olchowy C, Cebulski K, Łasecki M et al (2017) The presence of the gadolinium-based contrast agent depositions in the brain and symptoms of gadolinium neurotoxicity-a systematic review. PLoS One 12:1–14
3. Caroli A, Schneider M, Friedli I et al (2018) Diffusion-weighted magnetic resonance imaging to assess diffuse renal pathology: a systematic review and statement paper. Nephrol Dial Transplant 33:ii29–ii40
4. Panagiotaki E, Chan RW, Dikaios N et al (2015) Microstructural characterization of normal and malignant human prostate tissue with vascular, extracellular, and restricted diffusion for cytometry in tumours magnetic resonance imaging. Investig Radiol 50:218–227
5. Cheng L, Blackledge MD, Collins DJ et al (2016) T2-adjusted computed diffusion-weighted imaging: a novel method to enhance tumour visualisation. Comput Biol Med 79:92–98
6. Eisenberger U, Theony HC, Boesch C et al (2014) Living renal allograft transplantation : diffusion-weighted MR imaging in longitudinal follow-up of the donated and the remaining kidney. Radiology 270:800–808
7. Thoeny HC, De Keyzer F (2011) Diffusion-weighted MR imaging of native and transplanted kidneys. Radiology 259:25–38
8. Saritas EU, Lee JH, Nishimura DG (2011) SNR dependence of optimal parameters for apparent diffusion coefficient measurements. IEEE Trans Med Imaging 30:424–437
9. Zhang JL, Sigmund EE, Rusinek H et al (2012) Optimization of b-value sampling for diffusion-weighted imaging of the kidney. Magn Reson Med 67:89–97
10. Winfield JM, Tunariu N, Rata M et al (2017) Extracranial soft-tissue tumors: repeatability of apparent diffusion coefficient estimates from diffusion-weighted MR imaging. Radiology 284:88–99
11. Le Bihan D, Breton E, Lallemand D et al (1988) Separation of diffusion and perfusion in intravoxel incoherent motion MR imaging. Radiology 168:497–505
12. Ljimani A, Lanzman RS, Müller-Lutz A et al (2018) Non-gaussian diffusion evaluation of the human kidney by Padé exponent model. J Magn Reson Imaging 47:160–167
13. Jerome NP, D'Arcy JA, Feiweier T et al (2016) Extended T2-IVIM model for correction of TE dependence of pseudo-diffusion volume fraction in clinical diffusion-weighted magnetic resonance imaging. Phys Med Biol 61: N667–N680
14. Lemke A, Laun FB, Simon D et al (2010) An in vivo verification of the intravoxel incoherent motion effect in diffusion-weighted imaging of the abdomen. Magn Reson Med 64:1580–1585
15. Meeus EM, Novak J, Withey SB et al (2017) Evaluation of intravoxel incoherent motion fitting methods in low-perfused tissue. J Magn Reson Imaging 45:1325–1334
16. Vidić I, Jerome NP, Bathen TF et al (2019) Accuracy of breast cancer lesion classification using intravoxel incoherent motion diffusion-weighted imaging is improved by the inclusion of global or local prior knowledge with bayesian methods. J Magn Reson Imaging 50:1478–1488
17. Cho GY, Moy L, Zhang JL et al (2015) Comparison of fitting methods and b-value

sampling strategies for intravoxel incoherent motion in breast cancer. Magn Reson Med 74:1077–1085

18. Gurney-Champion OJ, Klaassen R, Froeling M et al (2018) Comparison of six fit algorithms for the intravoxel incoherent motion model of diffusionweighted magnetic resonance imaging data of pancreatic cancer patients. PLoS One 13:1–18
19. Jalnefjord O, Andersson M, Montelius M et al (2018) Comparison of methods for estimation of the intravoxel incoherent motion (IVIM) diffusion coefficient (D) and perfusion fraction (f). MAGMA 31(6):715–723. https://doi.org/10.1007/s10334-018-0697-5
20. Jerome NP, Boult JKR, Orton MR et al (2016) Modulation of renal oxygenation and perfusion in rat kidney monitored by quantitative diffusion and blood oxygen level dependent magnetic resonance imaging on a clinical 1.5T platform. BMC Nephrol 17:142
21. Jerome NP, Miyazaki K, Collins DJ et al (2016) Repeatability of derived parameters from histograms following non-Gaussian diffusion modelling of diffusion-weighted imaging in a paediatric oncological cohort. Eur Radiol 27:345–353
22. Orton MR, Jerome NP, Rata M, Koh D-M (2018) IVIM in the body: a general overview. In: Le Bihan D, Iima M, Federau C, Sigmund EE (eds) Intravoxel incoherent motion MRI Princ. Appl. Pan Stanford Publishing Pte. Ltd., pp 145–174
23. Kingsley PB (2006) Introduction to diffusion tensor imaging mathematics : part II. Anisotropy, diffusion- weighting factors, and gradient encoding schemes. Concepts Magn Reson Part A 28A:123–154
24. Kingsley PB (2006) Introduction to diffusion tensor imaging mathematics: part I. tensors, rotations, and eigenvectors. Concepts Magn Reson Part A 28A:101–122
25. Ding J, Chen J, Jiang Z et al (2016) Is low b-factors-based apparent diffusion coefficient helpful in assessing renal dysfunction? Radiol Med 121:6–11
26. Ding J, Chen J, Jiang Z et al (2016) Assessment of renal dysfunction with diffusion-weighted imaging: comparing intra-voxel incoherent motion (IVIM) with a mono-exponential model. Acta Radiol 57:507–512
27. Li Q, Wu X, Qiu L et al (2013) Diffusion-weighted MRI in the assessment of split renal function: comparison of navigator-triggered prospective acquisition correction and breath-hold acquisition. Am J Roentgenol 200:113–119
28. Prasad PV, Thacker J, Li LP et al (2015) Multi-parametric evaluation of chronic kidney disease by MRI: a preliminary cross-sectional study. PLoS One 10:1–14
29. Özçelik Ü, Çevik H et al (2017) Evaluation of transplanted kidneys and comparison with healthy volunteers and kidney donors with diffusion-weighted magnetic resonance imaging: initial experience. Exp Clin Transplant. https://doi.org/10.6002/ect.2016.0341
30. Friedli I, Crowe LA, Berchtold L et al (2016) New magnetic resonance imaging index for renal fibrosis assessment: a comparison between diffusion-weighted imaging and T1 mapping with histological validation. Sci Rep 6:1–15
31. Friedli I, Crowe LA, de Perrot T et al (2017) Comparison of readout-segmented and conventional single-shot for echo-planar diffusion-weighted imaging in the assessment of kidney interstitial fibrosis. J Magn Reson Imaging 46:1631–1640
32. Zhao J, Wang ZJ, Liu M et al (2014) Assessment of renal fibrosis in chronic kidney disease using diffusion-weighted MRI. Clin Radiol 69:1117–1122
33. Inoue T, Kozawa E, Okada H et al (2011) Noninvasive evaluation of kidney hypoxia and fibrosis using magnetic resonance imaging. J Am Soc Nephrol 22:1429–1434
34. Liu Z, Xu Y, Zhang J et al (2015) Chronic kidney disease: pathological and functional assessment with diffusion tensor imaging at 3T MR. Eur Radiol 25:652–660
35. Rona G, Pasaoglu L, Ozkayar N et al (2016) Functional evaluation of secondary renal amyloidosis with diffusion-weighted MR imaging. Ren Fail 38:249–255
36. Wang WJ, Pui MH, Guo Y et al (2014) 3T magnetic resonance diffusion tensor imaging in chronic kidney disease. Abdom Imaging 39:770–775
37. Emre T, Kiliçkesmez Ö, Büker A et al (2016) Renal function and diffusion-weighted imaging: a new method to diagnose kidney failure before losing half function. Radiol Med 121:163–172
38. Çakmak P, Yağci AB, Dursun B et al (2014) Renal diffusion-weighted imaging in diabetic nephropathy: correlation with clinical stages of disease. Diagnostic Interv Radiol 20:374–378
39. Palmucci S, Cappello G, Attinà G et al (2015) Diffusion weighted imaging and diffusion tensor imaging in the evaluation of transplanted kidneys. Eur J Radiol Open 2:71–80

40. Hueper K, Khalifa AA, Bräsen JH et al (2016) Diffusion-weighted imaging and diffusion tensor imaging detect delayed graft function and correlate with allograft fibrosis in patients early after kidney transplantation. J Magn Reson Imaging 44:112–121
41. Haque ME, Franklin T, Bokhary U et al (2014) Longitudinal changes in MRI markers in a reversible unilateral ureteral obstruction mouse model: preliminary experience. J Magn Reson Imaging 39:835–841
42. Hu G, Yang Z, Liang W et al (2019) Intravoxel incoherent motion and arterial spin labeling MRI analysis of reversible unilateral ureteral obstruction in rats. J Magn Reson Imaging 50:288–296
43. Togao O, Doi S, Kuro-o M et al (2010) Assessment of renal fibrosis with diffusion-weighted MR Imaging: study with murine model purpose: methods: results: conclusion. Radiology 255:772–780
44. Wang F, Takahashi KK, Li H et al (2018) Assessment of unilateral ureter obstruction with multi-parametric MRI. Magn Reson Med 79:2216–2227
45. Pons M, Leporq B, Ali L et al (2018) Renal parenchyma impairment characterization in partial unilateral ureteral obstruction in mice with intravoxel incoherent motion-MRI. NMR Biomed 31:1–9
46. Kaimori JY, Isaka Y, Hatanaka M et al (2017) Visualization of kidney fibrosis in diabetic nephropathy by long diffusion tensor imaging MRI with spin-echo sequence. Sci Rep 7:2–9
47. Yan YY, Hartono S, Hennedige T et al (2017) Intravoxel incoherent motion and diffusion tensor imaging of early renal fibrosis induced in a murine model of streptozotocin induced diabetes. Magn Reson Imaging 38:71–76
48. Jost G, Lenhard DC, Sieber MA et al (2011) Changes of renal water diffusion coefficient after application of iodinated contrast agents: effect of viscosity. Investig Radiol 46:796–800
49. Wang Y, Ren K, Liu Y et al (2017) Application of BOLD MRI and DTI for the evaluation of renal effect related to viscosity of iodinated contrast agent in a rat model. J Magn Reson Imaging 46:1320–1331
50. Liang L, Chen WB, KWY C et al (2016) Using intravoxel incoherent motion MR imaging to study the renal pathophysiological process of contrast-induced acute kidney injury in rats: comparison with conventional DWI and arterial spin labelling. Eur Radiol 26:1597–1605
51. Thoeny HC, Grenier N (2010) Science to practice: can diffusion-weighted MR imaging findings be used as biomarkers to monitor the progression of renal fibrosis? Radiology 255:667–668
52. Jerome NP, Orton MR, D'Arcy JA et al (2015) Use of the temporal median and trimmed mean mitigates effects of respiratory motion in multiple-acquisition abdominal diffusion imaging. Phys Med Biol 60:N9–N20
53. Wu CJ, Wang Q, Zhang J et al (2016) Readout-segmented echo-planar imaging in diffusion-weighted imaging of the kidney: comparison with single-shot echo-planar imaging in image quality. Abdom Radiol 41:100–108
54. He YL, Hausmann D, Morelli JN et al (2016) Renal zoomed EPI-DWI with spatially-selective radiofrequency excitation pulses in two dimensions. Eur J Radiol 85:1773–1777
55. Furuta A, Isoda H, Yamashita R et al (2014) Comparison of monopolar and bipolar diffusion weighted imaging sequences for detection of small hepatic metastases. Eur J Radiol 83:1626–1630
56. Kyriazi S, Blackledge M, Collins DJ, Desouza NM (2010) Optimising diffusion-weighted imaging in the abdomen and pelvis: comparison of image quality between monopolar and bipolar single-shot spin-echo echo-planar sequences. Eur Radiol 20:2422–2431
57. Clark CA, Hedehus M, Moseley ME (2001) Diffusion time dependence of the apparent diffusion tensor in healthy human brain and white matter disease. Magn Reson Med 45:1126–1129
58. Holland D, Kuperman JM, Dale AM (2010) Efficient correction of inhomogeneous static magnetic field-induced distortion in echo planar imaging. NeuroImage 50:175–183
59. Guyader J-M, Bernardin L, Douglas NHM et al (2015) Influence of image registration on apparent diffusion coefficient images computed from free-breathing diffusion MR images of the abdomen. J Magn Reson Imaging 42:315–330
60. Wetscherek A, Stieltjes B, Laun FB (2015) Flow-compensated intravoxel incoherent motion diffusion imaging. Magn Reson Med 74:410–419
61. Friedli I, Crowe LA, Viallon M et al (2015) Improvement of renal diffusion-weighted magnetic resonance imaging with readout-segmented echo-planar imaging at 3T. Magn Reson Imaging 33:701–708

62. Delalande C, De Zwart JA, Trillaud H et al (1999) An echo-shifted gradient-echo MRI method for efficient diffusion weighting. Magn Reson Med 41:1000–1008
63. Ding S, Trillaud H, Yongbi M et al (1995) High resolution renal diffusion imaging using a modified steady-state free precession sequence. Magn Reson Med 34:586–595
64. Lu L, Erokwu B, Lee G et al (2012) Diffusion-prepared fast imaging with steady-state free precession (DP-FISP): a rapid diffusion MRI technique at 7 T. Magn Reson Med 68:868–873
65. Lanzman RS, Ljimani A, Müller-Lutz A et al (2019) Assessment of time-resolved renal diffusion parameters over the entire cardiac cycle. Magn Reson Imaging 55:1–6